SUPERIOR SEAWORTHINESS OF A RESONANCE-FREE FAST OCEANGOING SWATH

(DOI No: 10.3940/rina.ijme.2014.a4.305)

M Yoshida, Kyushu University, Japan, **H Kihara**, National Defense Academy of Japan, Japan, **H Iwashita**, Hiroshima University, Japan, **M Kanda**, Akishima Laboratories (Mitsui Zosen) Inc., Japan and **T Kinoshita**, The University of Tokyo, Japan

SUMMARY

The speed reduction, additional resistance or slamming caused by the large amplitude ship motions, should be completely restricted for a large fast oceangoing ship because of the strict time-punctuality and the high value of the cargo. A "Resonance-Free SWATH (RFS)", which has negative restoring moments due to the extremely small water plane area, is introduced to minimize the motion responses. A motion control system using small fins is necessary for the RFS, which has no stability during high speed cruising. Theoretical estimations and experiments to search for the optimum values of PD control gains have been performed. Unsteady characteristics of fin-generated lift such as the time lag and the interaction among the fins and lower hulls have been measured and they are taken into account in the motion equations. Then, experiments using the RFS model with controlling fins have been carried out to validate the theoretical estimation for the motion responses of the RFS in waves. The theoretical and experimental results agree well with each other. The motion responses of the RFS in regular and irregular head waves are compared with those of other hull forms, such as a mono-hull, an ordinary SWATH and a trimaran. The clear advantage of the RFS regarding the seaworthiness has been found. In summary, the heave motion response of the RFS is reduced to 1/60 and the pitch motion becomes1/8, compared with those of the existing mono-hull ship.

NOMENCLATURE

A	Plane area of fin (m^2)
A_{ij}	Added mass (kg/kg m/kg m^2)
A_w	Water plane area (m^2)
α_{cj}	Attack angle of fin control (rad)
B	Breadth of ship (m)
B_{ij}	Damping coefficient (kg s^{-1}/kg m s^{-1}/kg m^2 s^{-1})
C_{ij}	Restoring force/moment (N m^{-1}/N/N m)
$C_{L\alpha}$	Lift-curve slope for attack angle (rad^{-1})
d	Draught (m)
E_i	Wave exciting force/moment (N/N m)
F_n	Froude number (-)
g	Acceleration of gravity (m s^{-2})
GM_L	Longitudinal metacentric height (m)
$H_{1/3}$	Significant wave height (m)
I	Inertia moment of ship (kg m^2)
K	Wave number (m^{-1})
K_{Pj}	Proportional gain to control j-th motion
K_{Dj}	Derivative gain to control j-th motion
L	Length of ship (m)
ℓ_0	Moment lever of fin (m)
λ	Wave length (m)
m	Mass of ship (kg)
m_0	0-th moment of power spectrum
R_{aw}	Added resistance in waves (N)
ρ	Density of water (kg m^{-3})
σ	Standard deviation
T_{01}	Mean wave period (s)
T, T_1, T_2	Time constant (s)
U	Ship speed (m s^{-1})
V	Displaced volume (m^3)
ω	Wave frequency (s^{-1})
ξ_j	Displacement in j-th motion (m/rad)
ζ_a	Amplitude of incident wave (m)

1. INTRODUCTION

The objective of this study is to present a conceptual design for a large fast oceangoing ship, which has a speed of 40 knots with a payload of 5,000-10,000 tonnes. It has especially good sea-keeping performance with no speed reduction and absolutely no slamming in waves of sea state 7 (significant wave height of 6-9 m). Due to the expected requirement of maintaining a precise navigation time schedule and a delicate handling for the fast ships to transport the high-valued cargo even in the rough sea, the speed reduction, additional resistance or slamming, caused by the large amplitude of the ship motions, should be restricted completely.

The development of fast ships in various hull forms such as a mono-hull [1], a catamaran [2], [3], a trimaran [4] and so on [5] has been attempted actively before. However, not with much significant success has been achieved in the reduction of the ship motion, especially including the effect of controlling fins. Furthermore, the value of quasi-steady state has been used as an approximation of the fin-generated lift [6], [7], [8], and the unsteady effects on the fin-generated lift have not been considered in most of studies regarding the simulation of the control system of the ship motions. When the control of the ship motions by means of the fins is discussed, the unsteady characteristics such as the time lag and the interaction among the fins and the lower hulls are very important [9], since they have a profound effect on the magnitude of the maximum control gain and the lift itself.

Firstly, in this study, a "Resonance-Free SWATH (RFS)" ship, which has negative restoring moments, is introduced as a hull form to minimize the ship motion responses [10]. Secondly, some experimental results and theoretical predictions regarding the hydrodynamic forces and moment acting on the RFS and its fins are presented. Thirdly, the optimum gains of a PD control, where P or D indicates the proportional or derivative control action respectively, and the motion responses of the RFS using small controlling fins are discussed. Especially, the unsteady lift characteristics such as the time lag and the interaction among the fins and the lower hulls are taken into account. Finally, the predominance of the RFS compared with other hull forms regarding the seaworthiness is demonstrated through the results of the experiments and the theoretical calculations.

2. CONCEPTUAL DESIGN OF RFS

2.1 DESIGN POLICY OF SHIP FORM

Comparing the motion amplitude between the ships with or without restoring force or moment, it is recognized that the latter one has no resonant peak and its response amplitude is smaller than the former one as illustrated in Figure 1. The ship without restoring moments can be realized by means of a SWATH with very small water plane area compared with the ordinary SWATH as shown in Figure 2. Consequently, the ship without the resonance of the motion responses is called a "Resonance-Free SWATH" and abbreviated as RFS in this study.

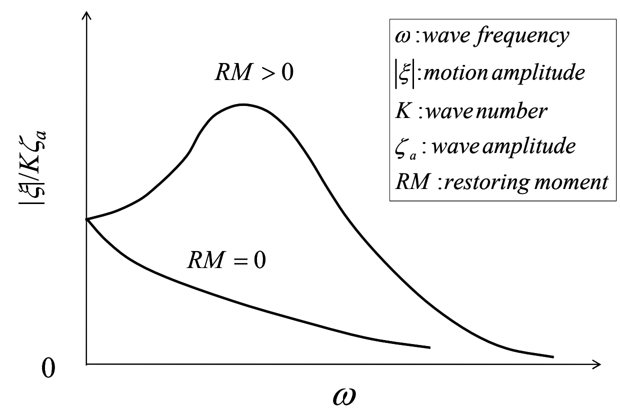

Figure 1: Resonance amplitude operator

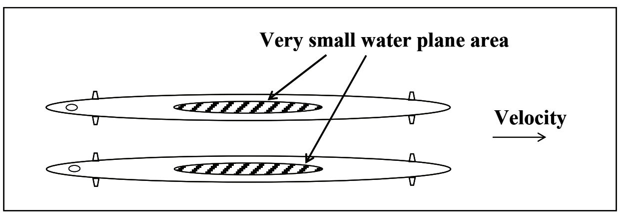

Figure 2: Schematic figure of water plane area of ship

2.2 ROUGH DESIGN OF RFS

An overall view of the rough conceptual design of the RFS [10], [11], [12] is shown in Figure 3. The RFS consists of five parts, i.e. one upper deck, two struts and two lower hulls. The upper deck is elevated out of the water at the speed of 28 knots when leaving the harbour and then the ship runs fast up to a high speed of 40 knots.

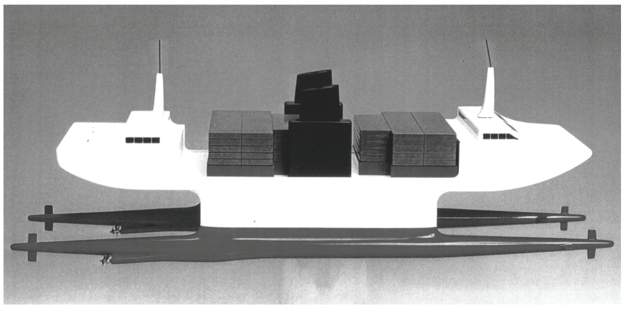

Figure 3: Rough design of Resonance-Free SWATH

As the RFS navigates across the ocean without the inherent self-stability, its motions have to be controlled using some special devices such as small fins attached to the lower hulls. On the other hand, the upper deck sinks back into the water when approaching the harbour and then the RFS runs at lower speed like an ordinary mono-hull ship with the inherent self-stability.

The resistance components of the RFS have been estimated as follows: Frictional resistance is determined using Schoenherr's coefficient for the equivalent flat plate. Wave-making resistance is estimated by means of Michell's thin ship theory for the strut and singularity distribution method for the lower hull. Viscous pressure resistance is considered as a correction term from sea trial of real ship. As a result, total resistance of the ship equals 810 tf at the cruising speed of 40 knots.

The calculation concerning the structural strength has been principally carried out under the condition of regular waves with a wave height of 10.8 m. This height represents the expected maximum value out of 1,000 waves of the sea state with a significant wave height of 6 m. Head and beam waves are selected as the designing wave directions. Normal and shear stresses acting on the three parts, i.e. the strut end of the lower hull (the root of the overhang portion of the lower hull), the upper deck connection (the central cross section of the upper deck) and the connecting part between the upper deck and the strut, have been calculated respectively. Where pitch moment, yaw moment, split force and split force moment due to the wave loads are considered as the calculation conditions. According to the calculation, the maximum principal stress is 24.4 kgf/mm^2, which is well within the acceptable limits for high strength steel with 70 kgf/mm^2 yield strength. The thickness of the plate at the lower hull is determined as 40 and 20 mm, while it is16 mm thick for the upper deck and 19 mm thick for the strut respectively.

Four pairs of controlling fins are installed near the bow and stern of the lower hulls. Each fin has an area of 20 mm^2

 ©2014: The Royal Institution of Naval Architects

respectively. To maintain the stability and the superior sea-keeping quality of the RFS effectively, these fins should operate below the water surface at all times in rough seas.

The conceptual design of the RFS is summarized as shown in Table 1. Additionally the height of the centre of gravity KG equals 18.54 m and the longitudinal metacentric height GM_L equals 0.03 m, almost zero. The RFS loads the cargo-carrying lighters on the deck, hence the deadweight includes the weight of these lighters. The unloading and loading of the lighters, the loading of fuel and the ship maintenance etc. are carried out during the short anchoring period. Accordingly, the RFS does not require any expensive cargo handling harbour facilities at the wharf. The RFS has the capability of crossing 4,800 nautical miles of Pacific Ocean in 5 days with a payload of 5,400 t at a high speed of 40 knots. The total engine power is 352,000 HP. At an initial glimpse, the transport efficiency of the RFS may not seem as good as that of an existing ship. However, when discussing the transport and economical efficiency of ocean-crossing, the comparison should be made among the existing ships, the RFS and the aircraft together. The economical efficiency of the RFS is much higher than that of the aircraft. From the aspect of the transport quality including the punctuality of transit time and the damages of cargo due to the slamming, the quality of the RFS is much better than that of the existing ships.

Table 1: Principal particulars of RFS

Displacement tonnage: 24,000 t
Light weight: 10,367 t
Power plants: 3,157 t
Dead weight: 13,633 t
Lighter: 1,000 t
Payload: 5,400 t, 540 containers (40 ft)
Fuel: 6,833 t
Upper hull: 200 m length, 55 m breadth
Lower hull: 230 m length, 8.85 m maximum diameter
Strut: 90 m length, 4.425 m maximum breadth
Draft: 12.85 m
Speed: 40 knots
Resistance: 810 tf
Main engine: 8 gas turbines (44,000 HP/turbine), total 352,000 HP
Propulsion: 8 contra-rotating propellers
Cruising distance: 4,800 nautical miles (Pacific Ocean)
Controlling fin: 8 fins, total fin area: 160 m^2

3. EXPERIMENTS AND CALCULATIONS

3.1 MODEL HULL FORMS

The experiments for four kinds of hull forms have been carried out in four model basins respectively. The measurements for the mono-hull model and the trimaran model have been carried out at Ocean Engineering Tank in Kyushu University while the experiments have been performed for the ordinary SWATH and the RFS models at Ocean Engineering Basin in The University of Tokyo. The RFS model has been retested at the Small and Large towing tanks of Akishima Laboratories (Mitsui Zosen).

The photographs of four ship models are shown in Figure 4. Also the principal particulars of four models are presented in Table 2 with items of length L, breadth B, draught d, longitudinal centre of buoyancy ℓ_{cb}, water plane area A_w, height of gravity centre KG, longitudinal metacentric height GM_L, radius of gyration κ_{yy}/L, mass ρV, advancing speed U or Froude number F_n where ρ indicates the density of water and V denotes the displaced volume of the model.

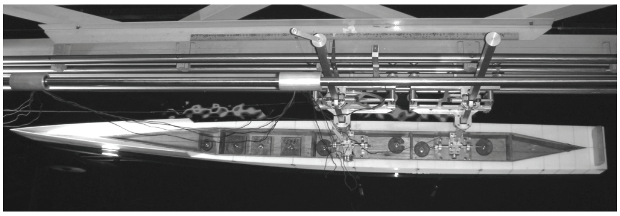

(a) Mono-hull model

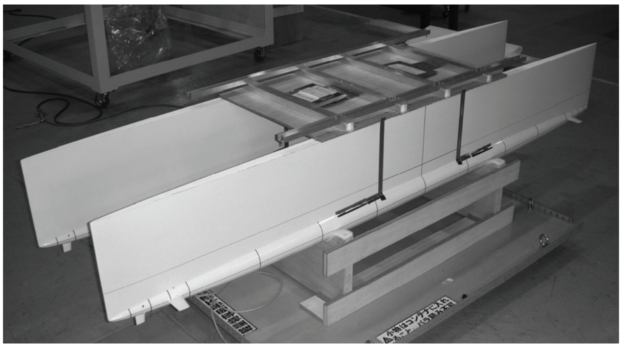

(b) Ordinary SWATH model

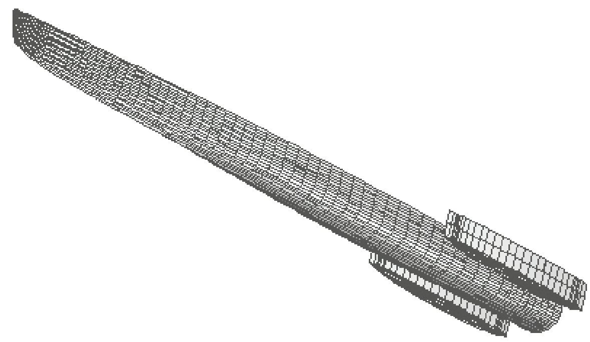

(c) Trimaran model

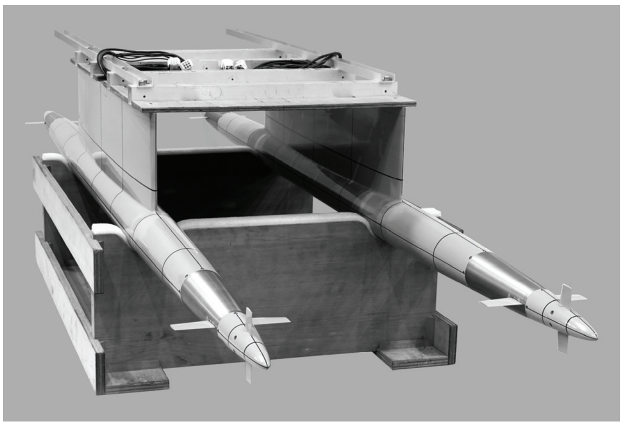

(d) RFS model

Figure 4: Overview of four kinds of model hull forms

Table 2: Principal particulars of four models

	Mono-hull	Ordinary SWATH	Trimaran	RFS
L (m)	2.5	2.0	2.5	2.0
B (m)	0.192	0.486	0.192	0.486
d (m)	0.064	0.112	0.064	0.112
ℓ_{cb} (%)	+ 8.96	0	---	0
A_w (m^2)	0.3503	0.1208	---	0.0473
KG (m)	0.084	0.189	---	0.180
GM_L (m)	8.607	1.480	---	− 0.019
κ_{yy}/L	0.192	0.228	---	0.207
ρV (kg)	14.71	18.68	---	15.49
U (m/s)	2.476	1.918	2.476	1.918
F_n	0.50	0.433	0.50	0.433

ℓ_{cb} : + is taken aftward.

The RFS model consists of one upper deck, two struts and twin lower hulls as shown in Figure 5. The cross section of the lower hull is circular with the maximum diameter of 0.077 m. The horizontal cross section of the strut is elliptical with a length of 0.783 m and the maximum breadth of 0.0385 m. The height of the strut is approximately 0.154 m. The longitudinal metacentric height GM_L equals −0.019 m. Four pairs of horizontal controlling fins and two pairs of vertical rudders are attached to the lower hulls. Each fin has the following configuration: plane area A= 0.001518 m^2, chord length c=0.0357 m (base side) or 0.0278 m (tip side), span s=0.0478 m, aspect ratio s^2/A=1.51 and the symmetrical wing profile of NACA0012.

The ordinary SWATH and the RFS models have the same upper deck and lower hulls but different strut length. The strut length of the ordinary SWATH model is equal to 2.0 m, which is approximately three times as long as the strut length 0.783 m of the RFS model. Consequently, both models have different parameters of A_w, GM_L, ρV and so on.

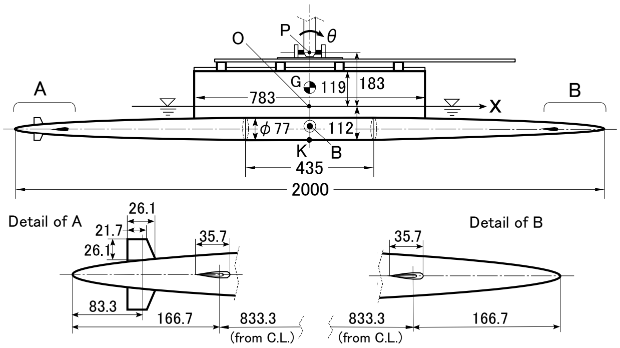

(a) Side view

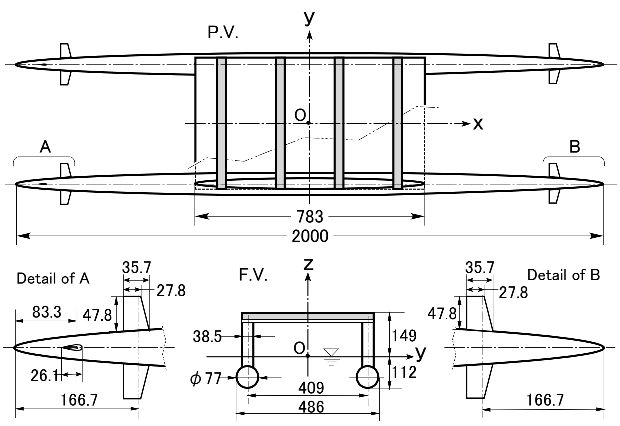

(b) Plane and front view

Figure 5: Plan of RFS model (unit: mm)

3.2 MOTION CONTROL SYSTEM

The assembling drawing of the controlling fins is shown in Figure 6. The four sets of fin controlling equipment are installed in the bow and stern ends of both lower hulls, where the diameter of the lower hull is about 40 mm. The controlling equipment consists of DC servomotor, worm gear, fin axis and potentiometer principally. The attack angle of four pairs of movable fin equipment can be controlled independently. The maximum amplitude of the attack angle of each fin is limited to 20 deg, and the maximum frequency of fin oscillation equals 3.0 Hz.

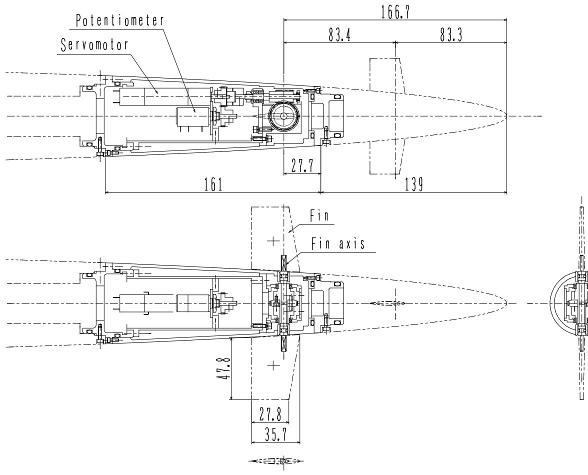

Figure 6: Assembly of controlling fins (unit: mm)

The block diagram of the fin control system used in the experiments is shown in Figure 7. The phase lag of the fin control system between the output value of potentiometer (the feedback signal of the heave or pitch motion) and the output value of fin actuator (the actual attack angle) has been measured. In the case that the fin rotating frequency is 1.105 Hz (corresponds to λ/L=2.00), the lag equals about 26 deg which is equivalent to the time delay of about 0.07 s in the control system. This value of the system is appropriate and problem-free to control the motion responses delicately.

©2014: The Royal Institution of Naval Architects

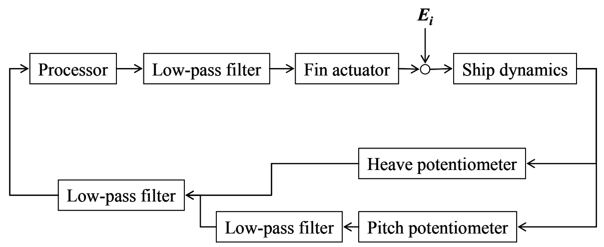

Figure 7: Block diagram of fin control system

3.3 EXPERIMENTAL CONDITIONS

Four kinds of tests have been carried out; forced oscillation tests in still water, restrained tests in waves, the measurements of the fin-generated lift in still water and free motion tests in waves.

Froude number, defined as $F_n = U/\sqrt{gL}$ with towing speed U and gravity acceleration g, is 0.50 for the mono-hull and the trimaran models, and is 0.433 for the ordinary SWATH and the RFS models. The adopted Froude number is common in all the four kinds of tests. There seems to be a slight difference among the values of Froude number for the four models in comparison. However, the tendency of the magnitude of the hydrodynamic forces or the motion responses can be compared adequately in the high-speed region according to the study of TAKARADA et al. [1]. For the forced oscillation tests, oscillating frequencies are changed in a range of KL=2-40, where K denotes the wave number. For the restrained tests in waves to measure the wave exciting forces, the wave length varies in a range of λ/L = 0.4-4.0. In the forced oscillation tests and the restrained tests for the RFS model, the attack angle of eight fins is fixed at zero degree relative to the longitudinal hull axes. For the tests of measuring the fin-generated lift using the RFS model, the model hull is fixed, and the fore and aft fins rotate in a frequency range of ω = 0-20 rad/s with the rotating amplitude of 10 deg respectively. In the mode to control the heave motion, both fore and aft fins rotate in the same phase, while in the mode to control the pitch motion, they rotate in the inverse phase. For the free motion tests in waves, experimental conditions are the same as those in measuring the wave exciting forces except for the rotation of the fins. All tests have been carried out in head sea conditions. Because it is considered that the head sea condition provides the most severe state for the ship motions [1].

3.4 THEORETICAL CALCULATIONS

A Cartesian coordinate system O-xyz that follows ship forward speed U is adopted to describe the problem as shown in Figure 5. The O-xy plane coincides with the undisturbed free surface while the z axis is pointing upward and passes through the gravity centre G of the RFS model.

Frequency-domain 3D Rankine panel method (RPM) [13] based on the potential theory has been adopted to estimate the hydrodynamic forces and ship motions for the mono-hull and the trimaran models. Furthermore strip method [14] has been applied to calculate the hydrodynamic forces for the ordinary SWATH and the RFS models and to calculate the ship motions for the ordinary SWATH. The viscous effect of the lower-hulls and fins, as well as the fin-generated lift, is considered in the calculation for the ordinary SWATH and the RFS models, based on the correction method by Lee [6]. Also the interaction of the hydrodynamic forces among two lower hulls is considered [14].

4. HYDRODYNAMIC FORCES AND MOMENTS

4.1 ADDED MASS AND DAMPING COEFFICIENTS

Hydrodynamic forces and moments, measured in the forced oscillation tests of pure heave or pure pitch motion in still water, are shown in Figure 8 and Figure 9. The coefficient A_{ij} or B_{ij} denotes the added mass or the damping coefficient, respectively, in the i-th direction induced by the motion of j-th direction. They are normalized by the mass ρV or the product of the mass and the circular frequency ω etc, respectively. Figure 8 shows the results in pure heaving or pitching direction. On the other hand, Figure 9 shows the results in coupled terms between heaving and pitching motions. The experimental results of the mono-hull, the trimaran and the RFS models are plotted in the figures. Also the calculated results by the use of RPM for the mono-hull and the trimaran models or by the use of strip method for the RFS model are plotted in the same figures. The experimental results of A_{33} and A_{55} of the RFS shown in Figure 8 are small compared with those of the mono-hull and the trimaran because the hull form of the RFS is considerably slender compared with that of the mono-hull or the trimaran. Also, the experimental results of B_{33} in pure heaving motion for the RFS are smaller than those for the mono-hull or the trimaran, while the magnitude of B_{55} in pure pitching motion for the RFS is larger than that for the mono-hull or the trimaran. The effect on reducing the pitching motion for the RFS can be expected especially by the fin because of the large lever of pitching moment in spite of the small fin area. In Figure 8 and Figure 9, the calculated results of each model coincide with the experimental results properly or explain the tendency of those.

4.2 WAVE EXCITING FORCE AND MOMENT

The measured results of the amplitude and the phase difference of the wave exciting force and moment acting on various models are presented in Figure 10. $|E_i|$ denotes the amplitude of the force or moment in i-direction, and ζ_a is the amplitude of the incident waves as used in the figure. Also the calculated results by the use of RPM or strip method for each model are plotted. It is observed that the calculated results for each model coincide well

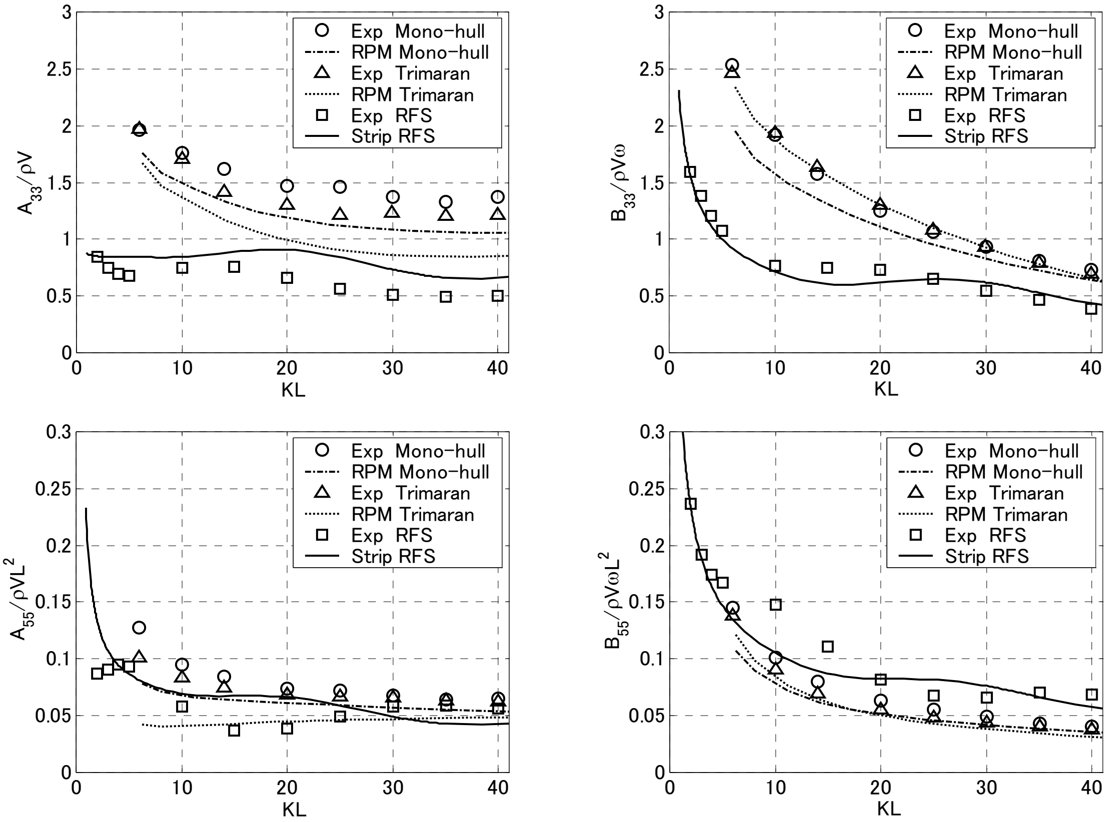

Figure 8: Added mass and damping coefficients for heave and pitch

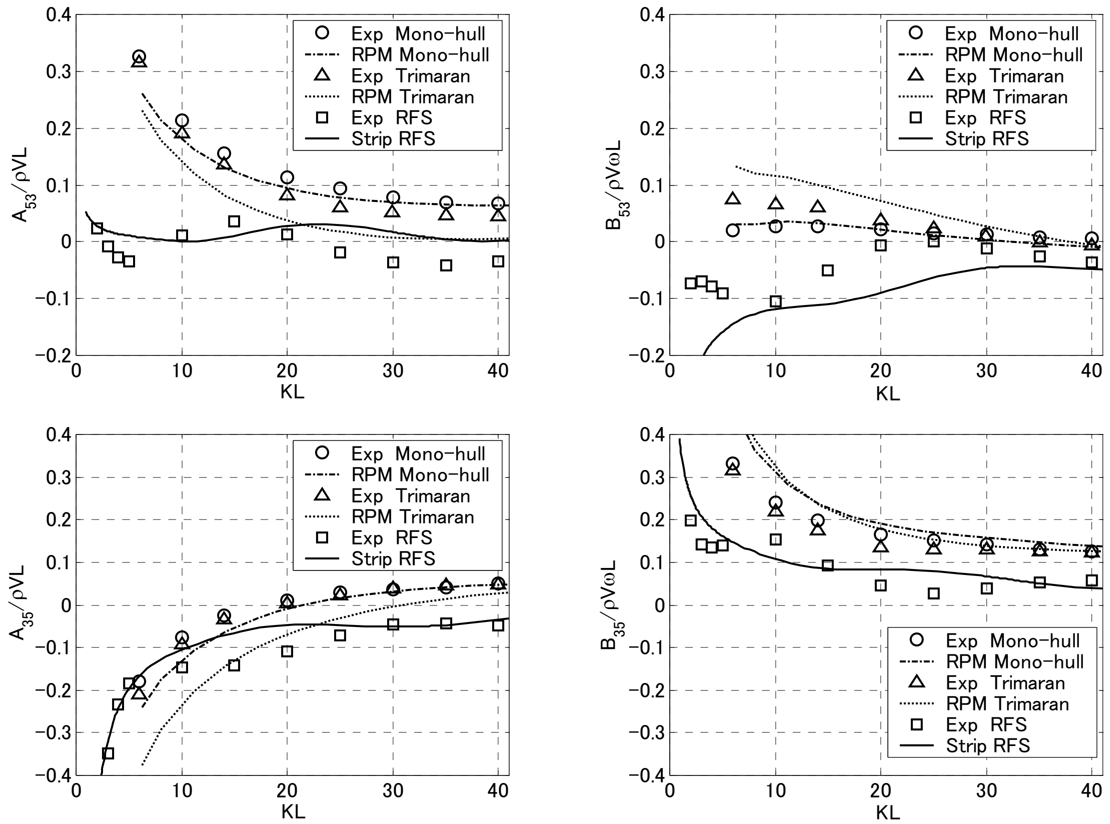

Figure 9: Coupled added mass and damping coefficients between heave and pitch

©2014: The Royal Institution of Naval Architects

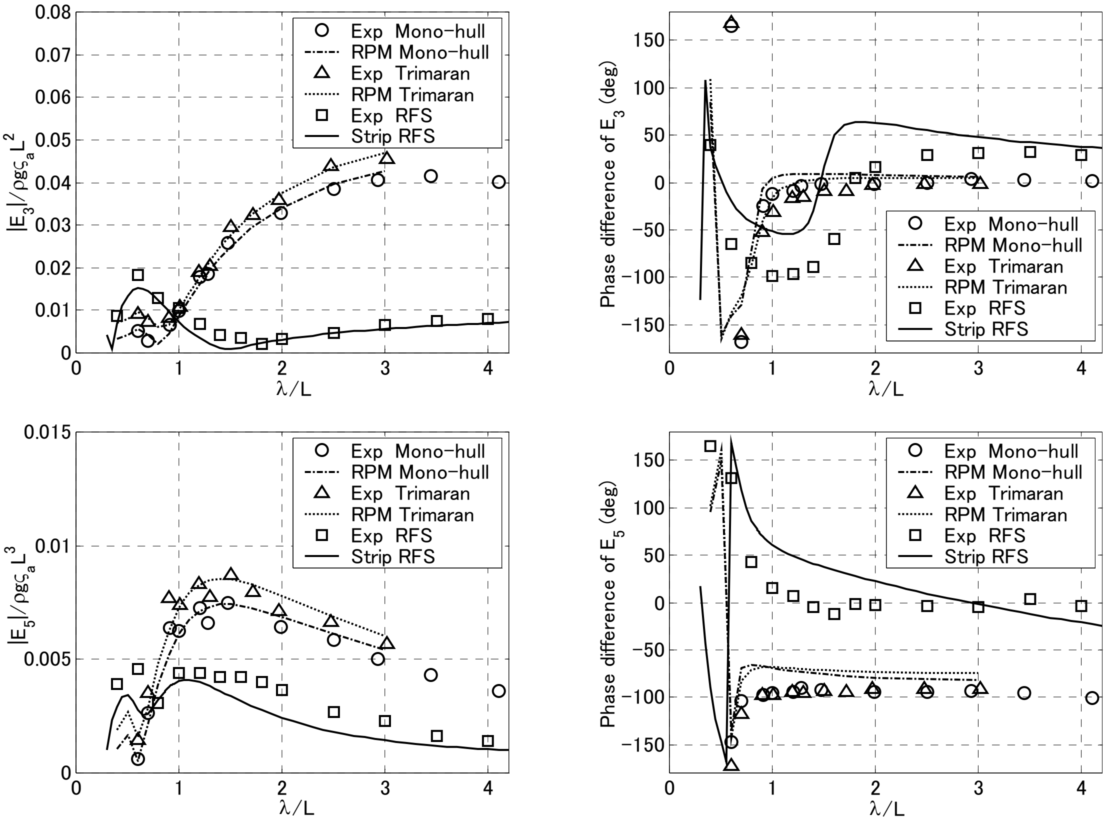

Figure 10: Wave exciting force and moment

with the measured results. The experimental results of the amplitude of the wave exciting force $|E_3|$ and moment $|E_5|$ in the case of the RFS are small compared with the case of the mono-hull or the trimaran.

4.3 UNSTEADY CHARACTERISTICS OF FIN-GENERATED LIFT

The experimental results of measuring the fin-generated lift for the RFS model are presented in Figure 11 and Figure 12. In Figure 11, $C_{L\alpha 3}$ indicates the lift-curve slope with respect to the attack angle operated in the heave control mode while $C_{L\alpha 5}$ denotes that in the pitch control mode. In Figure 12, $C_{L\alpha}$ indicates the lift-curve slope of each fore or aft fin in the case that the fore or aft fin rotates one by one. The unsteady characteristics of the fin-generated lift such as the time lag of generating lift (i.e. the phase lag) and the interaction among the fore fins, the aft fins, the struts and the lower hulls are shown in these figures. As a whole, the amplitude of the lift-curve slope gets smaller slightly and the phase lag becomes larger as the frequency ω increases. This is the feature, which is generally as predicted. Considering these figures in detail, it can be seen as follows. In Figure 11, the amplitude of the lift-curve slope of the aft fin has periodical fluctuation in both cases of the heave and pitch control modes, while there exists no fluctuation for that of the fore fin. Also, as regarding the phase lag, there seems to be same feature. It is understood that the lift-generation of the aft fin is affected by the fore fin in general. This phenomenon is confirmed from Figure 12, which shows that the fore fin does not affect the amplitude or the phase lag of the lift generated by the aft fin when the only aft fin rotates. Furthermore, there seems to be inverse feature regarding the hollow and hump of the periodic fluctuation in the amplitude and the phase lag of the lift-curve slope when comparing the control modes of heave and pitch.

Now, considering the lift-curve slope for the attack angle in the steady state, it is expressed as

$$C_{L\alpha} = (k_{W(B)} + k_{B(W)})(C_{L\alpha})_W \tag{1}$$

based on the body-fin effect [6], [15], where

$$k_{W(B)} = \frac{(C_{L\alpha})_{W(B)}}{(C_{L\alpha})_W},\ k_{B(W)} = \frac{(C_{L\alpha})_{B(W)}}{(C_{L\alpha})_W} \tag{2}$$

in which the subscript W represents the case of the fin alone, $B(W)$ the case of the lift on the body induced by the fin, and $W(B)$ the case of the lift on the fin induced by the body. For low aspect ratio wings, $(C_{L\alpha})_W$ is evaluated by Whicker and Fahlner [16] as

$$(C_{L\alpha})_W = \frac{1.8\pi A_e}{1.8 + \sqrt{A_e^{\,2} + 4}} \quad \text{per radian} \tag{3}$$

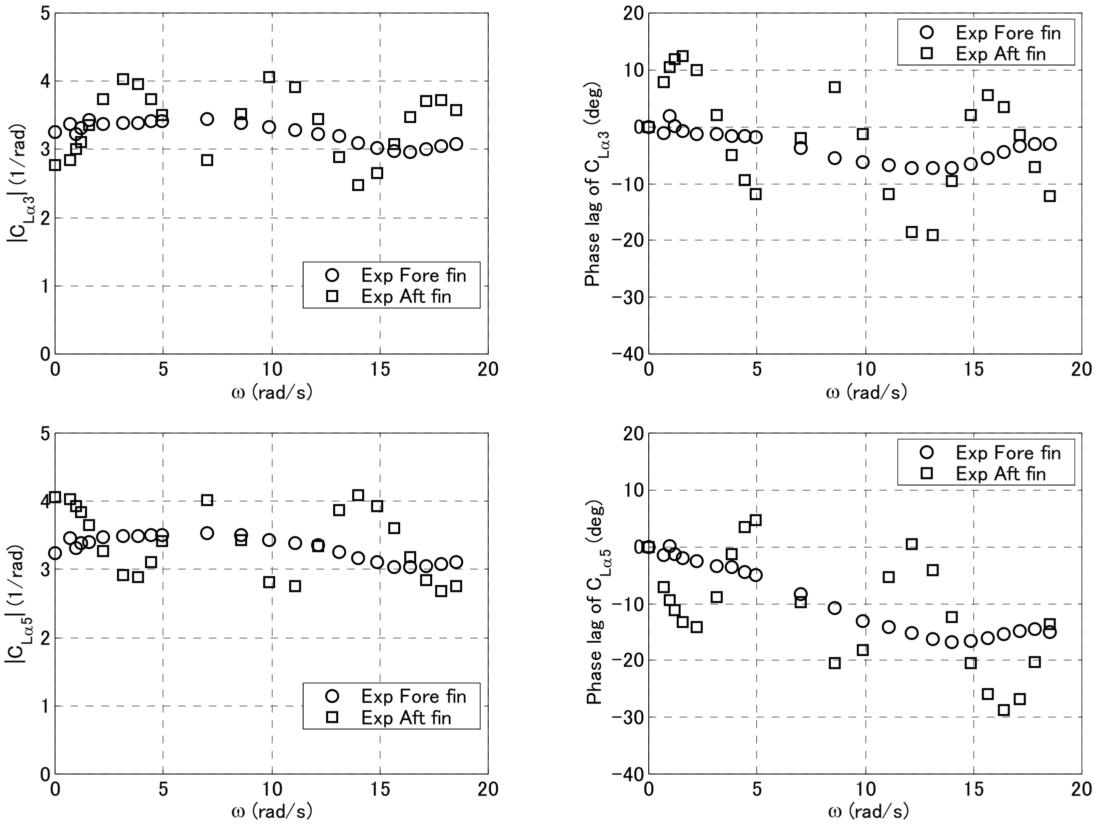

Figure 11: Unsteady characteristics of lift acting on fore or aft fin

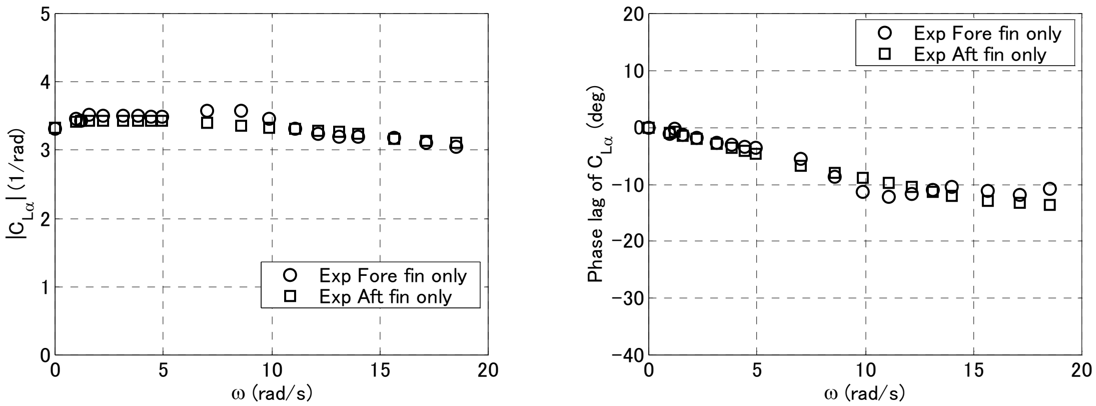

Figure 12: Unsteady characteristics of lift in the case that fore or aft fin operates one by one

and

$$A_e = (r_0 - \frac{r^2}{r_0}) \,/\, c \tag{4}$$

where A_e is the effective aspect ratio, r indicates the radius of the body, r_0 denotes the transverse distance from the body axis to the tip of the fin and c represents the average chord length of the fin.

As r is 0.02375 m, r_0 is 0.07155 m and c is 0.0318 m in the case of the RFS model, it is obtained A_e = 2.0 and then $(C_{L\alpha})_W$ = 2.44. Also $k_{W(B)}$ or $k_{B(W)}$ equals 0.93 or 0.35 respectively in accordance with the study of Pitts et al. [15]. Accordingly, the lift-curve slope in the quasi-steady state, $C_{L\alpha}$, is calculated as 3.12 from Equation (1).

On the other hand, in Figure 11, it can be found that $C_{L\alpha}$ becomes approximately 3.2 when the frequency close in on the steady state ω = 0, especially in the case of the fore fins. This fact shows that the estimation of the fin-generated lift by means of aerodynamics theory works well in the present hydrodynamic experiment.

 ©2014: The Royal Institution of Naval Architects

5. PD CONTROL OF RFS MOTION

5.1 MOTION EQUATIONS

The equations of coupled motion in heave z and pitch θ directions including the controlling forces and the time lag of the control system are shown as follows:

$$
\left\{
\begin{aligned}
&(m+A_{33})\,\ddot{z}+B_{33}\,\dot{z}+C_{33}\,z+A_{35}\,\ddot{\theta}+B_{35}\,\dot{\theta}+C_{35}\,\theta \\
&\qquad\qquad = E_3+F_{33}\,\alpha_{c3}+F_{35}\,\alpha_{c5} \\
&(I+A_{55})\,\ddot{\theta}+B_{55}\,\dot{\theta}+C_{55}\,\theta+A_{53}\,\ddot{z}+B_{53}\,\dot{z}+C_{53}\,z \\
&\qquad\qquad = E_5+F_{55}\,\alpha_{c5}+F_{53}\,\alpha_{c3} \\
&T_1\,\ddot{\alpha}_{c3}+T_2\,\dot{\alpha}_{c3}+\alpha_{c3}=(K_{D3\alpha}\,\dot{z}+K_{P3\alpha}\,z) \\
&T_1\,\ddot{\alpha}_{c5}+T_2\,\dot{\alpha}_{c5}+\alpha_{c5}=(K_{D5\alpha}\,\dot{\theta}+K_{P5\alpha}\,\theta)
\end{aligned}
\right. \tag{5}
$$

where controlling targets are z=0 and θ=0, m indicates the mass of the model, I denotes the inertia moment, A_{ij}, B_{ij} and C_{ij} are the added mass, the damping coefficient and the restoring force or moment respectively, E_i is the wave exciting force or moment, F_{ij} describes the characteristic of the lift, α_{cj} indicates the attack angle of the fin to control the motion, T_1, T_2 describe the dynamic characteristics of second order time lag in the fin control system and $K_{Pj\alpha}$ or $K_{Dj\alpha}$ denotes P or D control gain constant which is reduced to attack angle base as shown in the following equations.

$$
\left\{
\begin{aligned}
&F_{33}=F_{33f}+F_{33a} \\
&F_{53}=-F_{33f}\,\ell_f-F_{33a}\,\ell_a \\
&F_{55}=-F_{55f}+F_{55a} \\
&F_{35}=\frac{F_{55f}}{\ell_f}-\frac{F_{55a}}{\ell_a}
\end{aligned}
\right. \tag{6}
$$

and

$$
\left\{
\begin{aligned}
&F_{33f,a}=-\frac{1}{2}\rho A_{f,a}C_{L\alpha 3f,a}C_{3f,a}(\omega)U^2 \\
&F_{55f,a}=\frac{1}{2}\rho A_{f,a}C_{L\alpha 5f,a}C_{5f,a}(\omega)U^2\ell_{f,a}
\end{aligned}
\right. \tag{7}
$$

where

$$
C_{jf,a}(\omega)=C_{cjf,a}(\omega)+i\,C_{sjf,a}(\omega) \tag{8}
$$

and subscript f or a indicates the fore or aft fin, the symbol $\ell_{f,a}$ denotes the x-coordinate of the axis point (approximately quarter-chord point) of the fore or aft fin, ρ is the density of water, $A_{f,a}$ is total fin area of the fore or aft fin, U indicates the ship speed. Also, $C_{L\alpha jf,a}$ denotes the quasi-steady lift-curve slope of the fore or aft fin in the heave or pitch motion control respectively and $C_{jf,a}$ describes the interaction among the fins and the lower hulls, and the time lag of the lift generation. It is observed that the feature of Equation (8) is confirmed by the results shown in Figure 11.

The condition of fin control is that the attack angle of the fore or aft fin is of the same magnitude in the same direction for the heave motion control while it is of the same magnitude but in the inverse direction for the pitch motion control.

As a summary of the above description, the controlling forces due to the fin-generated lift, the time lag and the interaction among the fins and the lower hulls regarding the fin-generated lift, and the time lag of whole control system are considered in the motion equation. In Equation (5), the values of the lift-curve slope are given by the characteristics shown in Figure 11.

Generally, P control gain in the control system works to shift the resonant frequency while D gain contributes to reduce the amplitude of the ship motions over the whole range of the frequency when referring to the curve of response amplitude operator as shown in Figure 1. As one of the most commonly used form of feedback control, PD control has been adopted in the present study due to its simplicity, because the present study seeks to minimize the variation of unsteady ship motion in waves.

5.2 CONTROL BLOCK DIAGRAM

The Laplace transform of Equation (5) is given as follows:

$$
\left\{
\begin{aligned}
&H_{33}\,Z(s)+H_{35}\,\Theta(s)=\mathrm{E}_3(s)+F_{33}\mathrm{A}_{c3}(s)+F_{35}\mathrm{A}_{c5}(s) \\
&H_{55}\,\Theta(s)+H_{53}\,Z(s)=\mathrm{E}_5(s)+F_{55}\mathrm{A}_{c5}(s)+F_{53}\mathrm{A}_{c3}(s) \\
&(T_1s^2+T_2s+1)\,\mathrm{A}_{c3}(s)=(K_{D3\alpha}s+K_{P3\alpha})\,Z(s) \\
&(T_1s^2+T_2s+1)\,\mathrm{A}_{c5}(s)=(K_{D5\alpha}s+K_{P5\alpha})\,\Theta(s)
\end{aligned}
\right. \tag{9}
$$

and

$$
H_{ij}=(m_{ij}+A_{ij})\,s^2+B_{ij}\,s+C_{ij} \tag{10}
$$

where Z, Θ, E_i, A_{cj} are the corresponding Laplace transform of z, θ, E_i, α_{cj} and m_{ij} indicates the mass matrix. The block diagram of this multi-input multi-output (MIMO) control system is expressed in Figure 13, where

$$
G_{ij}=F_{ij}\,\frac{K_{Dj\alpha}\,s+K_{Pj\alpha}}{T_1\,s^2+T_2\,s+1} \tag{11}
$$

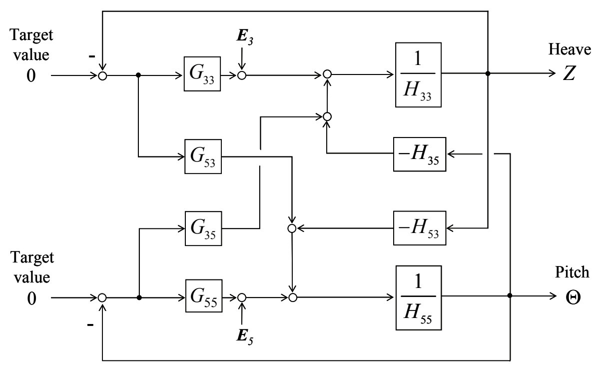

Figure 13: Control block diagram

Now, there are two steps to be made to obtain the open-loop transfer function of the control system, i.e. Step 1: Control system is regarded as a single-input single-output (SISO) system in which only pitch control works without any control on the heave motion. Stability of P and D gain constants (K_{P5}, K_{D5}) are discriminated by the use of a Bode plot to obtain the optimum or maximum stable values of those gain constants for pitch. Step 2: Heave and pitch motions are both controlled. Pitch gain constants K_{P5} and K_{D5} determined in step 1 are fixed, and the pitch control system is regarded as closed-loop. Then the Bode plot can be traced by the use of the open-loop transfer function and the optimum or maximum stable values of heave gain constants K_{P3} and K_{D3} are determined.

The effects of the hydrodynamic force coefficients $A_{ij}(\omega)$, $B_{ij}(\omega)$ and the wave exciting forces $E_i(\omega)$, which depend on the angular frequency ω of the motions, are included in the calculation of a Bode plot.

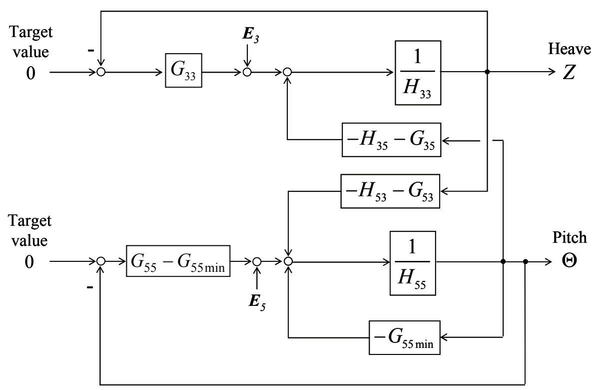

Figure 14: Control block diagram of ship without restoring moment

As the expression of G_{55min} or G_{55}-G_{55min} means that a part of input gain K_{P5} is applied as the minimum pitch P gain K_{P55min} to replace the inherent negative restoring moment of the RFS, the block diagram in Figure 13 is rewritten to that shown in Figure 14. The open-loop transfer functions P_5 of step 1 and P_{35} of step 2 are calculated as follows:

$$P_5 = \frac{(G_{55} - G_{55\min})H_{33}}{(H_{55} + G_{55\min})H_{33} - (H_{35} + G_{35})(H_{53} + G_{53})} \quad (12)$$

$$P_{35} = \frac{G_{33}\,(G_{55} + H_{55})}{H_{33}\,H_{55} - (H_{35} + G_{35})(H_{53} + G_{53}) + H_{33}\,G_{55}} \quad (13)$$

5.3 SIMULATION USING BODE PLOT

According to the findings from the previous study [12] that the effect of D gain is much more important than that of P gain, the minimum P gain constant and the maximum D gain constant should be adopted for the PD control of the RFS motions. Then, these gain constants must be stable in the control system.

Table 3: Predicted maximum stable D gain for RFS model

	P control	D control
Heave	K_{P3}=0 kg/s^2	K_{D3}=214 kg/s
Pitch	K_{P5}=99 kgm^2/s^2	K_{D5}=112 kgm^2/s

The minimum P gain can be decided as follows: Firstly, for the heave motion control, P gain constant is fixed as K_{P3}=0, because there exists a small restoring force (reserved buoyancy) C_{33}=464.0 N/m in real ship scale and there is no natural disturbance force in the heave direction. Next, for the pitch motion control, total value of K_{P5}=1.74*10^{10} kgm/s^2 in real ship scale or 99 kgm/s^2 in model scale is assigned, which includes the values of the negative restoring moment, i.e. the Munk moment when running at F_n=0.433 and the restoring moment at a gust of wind is required for the minimum P gain. Then, the maximum stable D gain is searched for in accordance with two steps as shown in section 5.2. Finally, the calculations or the experiments of the motion responses are carried out, and then the results should be checked to see whether the attack angle of all the fins has been kept below the stall angle. To discriminate by means of a Bode plot, the gain margin = 10 dB and the phase margin = 60 deg are assumed just for the sake of safety. The maximum stable D gain predicted for the RFS model is shown in Table 3 from the result of the search using a Bode plot.

5.4 MAXIMUM STABLE 'D' GAIN

The theoretical estimation using a Bode plot has been followed by experiments searching for the maximum stable D gain. In the control system as shown in Figure 7, the value $\alpha_{cf,a}$ of the attack angle instructed to the fin is calculated according to the following Equation.

$$\alpha_{cf,a} = \alpha_{c3f,a} \mp \alpha_{c5f,a} = \frac{K_{D3}\dot{z} + K_{P3}z}{4\rho AC_{L\alpha}U^2} \mp \frac{K_{D5}\dot{\theta} + K_{P5}\theta}{4\ell_0\rho AC_{L\alpha}U^2} \quad (14)$$

where the sign on the right-hand side of Equation (14) is − at the fore fin (abbreviated as f) or + at the aft fin (abbreviated as a), $C_{L\alpha}$ indicates the lift-curve slope (=3.12 1/rad) and ℓ_0 denotes the moment lever of the fin (=0.8333 m). Following the discussion in section 4.3, the fixed value of $C_{L\alpha}$ =3.12 has been adopted in the experiments of motion-control by PD gain.

The impulse response experiments of the RFS model with controlling fins have been carried out at F_n=0.433 in still water. The discriminant of the maximum stable D gain has been performed through the systematic tests. The model starts to run at a pitch attitude of θ= + or −2 deg. During the tests, it is checked whether the model can be controlled well and the attitude can be kept horizontal when running at F_n=0.433. In practice, the failure of the control

 ©2014: The Royal Institution of Naval Architects

system is not only caused by the problem of divergence but also by the hunting problem. The latter one is a phenomenon relating to the high frequency oscillation of controlling fins. The maximum stable D gain is usually decided at the turning point of the hunting.

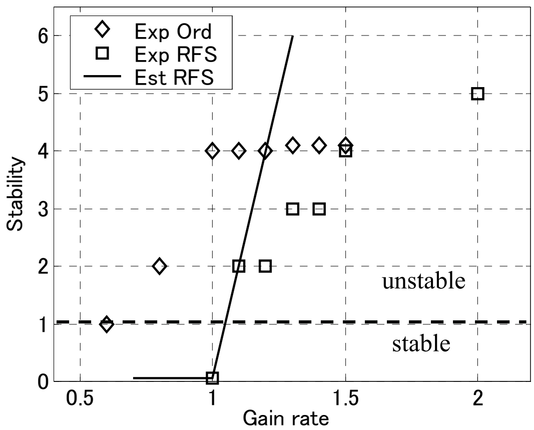

Figure 15: Maximum stable gain for ordinary SWATH or RFS

Table 4: PD gain for ordinary SWATH or RFS

	Heave		Pitch	
	K_{P3} (kg/s^2)	K_{D3} (kg/s)	K_{P5} (kgm^2/s^2)	K_{D5} (kgm^2/s)
Ord-OGA	0	128.4	0	67.2
RFS-GA	0	214	99	112

Table 5: Values of D gain for ordinary SWATH

	Heave		Pitch	
	K_{P3} (kg/s^2)	K_{D3} (kg/s)	K_{P5} (kgm^2/s^2)	K_{D5} (kgm^2/s)
Ord-OGA	0	128.4	0	67.2
Ord-OGC2	0	171.2	0	89.6
Ord-OGC	0	214	0	112

Table 6: Values of D gain for RFS

	Heave		Pitch	
	K_{P3} (kg/s^2)	K_{D3} (kg/s)	K_{P5} (kgm^2/s^2)	K_{D5} (kgm^2/s)
RFS-GB	0	107	99	56
RFS-GA	0	214	99	112
RFS-GC	0	256.8	99	134.4

Table 7: Values of P gain for RFS

	Heave		Pitch	
	K_{P3} (kg/s^2)	K_{D3} (kg/s)	K_{P5} (kgm^2/s^2)	K_{D5} (kgm^2/s)
RFS-GA	0	214	99	112
RFS-GD2	0	214	198	112
RFS-GDF	0	214	235	112
RFS-GD3	0	214	297	112

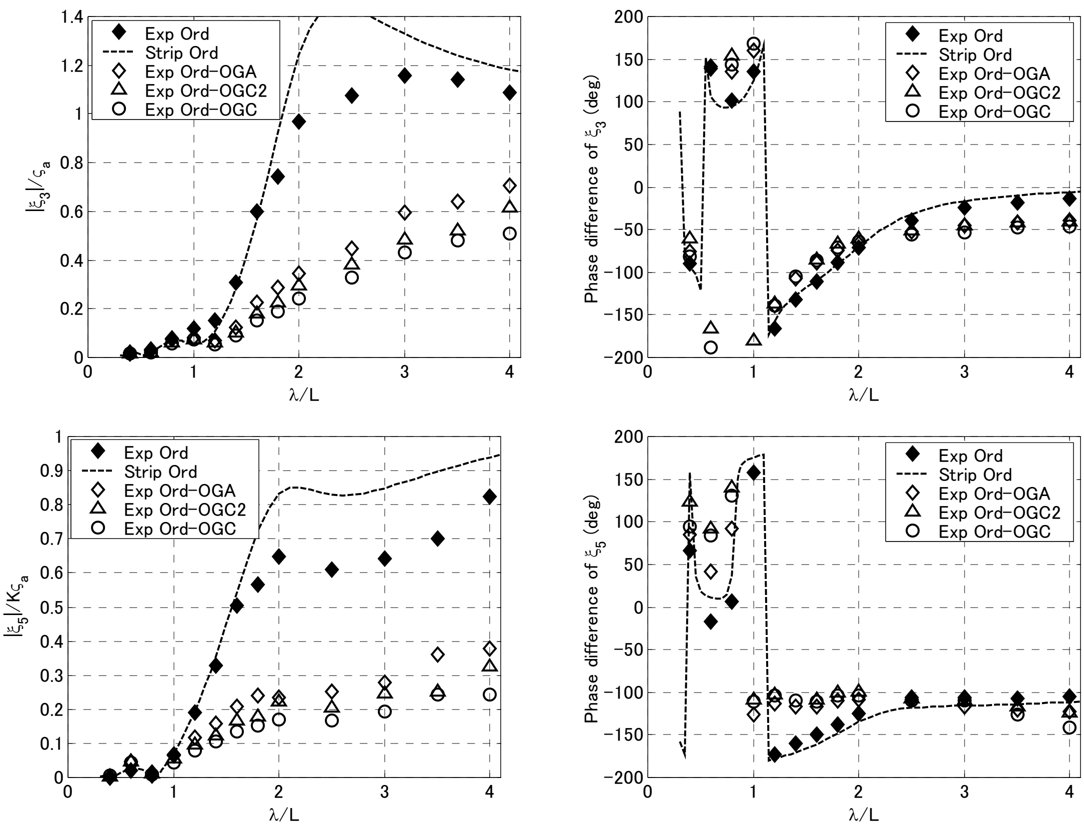

Figure 16: Effect of D gain on motion responses of ordinary SWATH in regular head waves

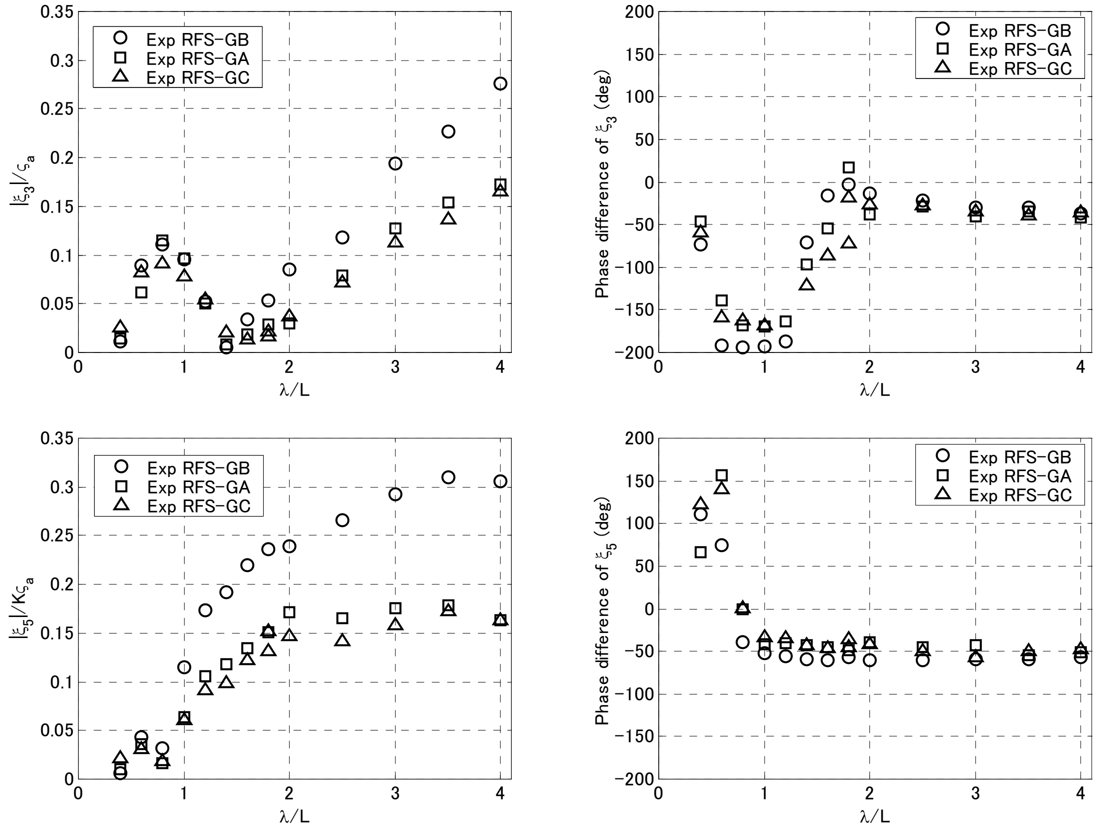

Figure 17: Effect of D gain on motion responses of RFS in regular head waves

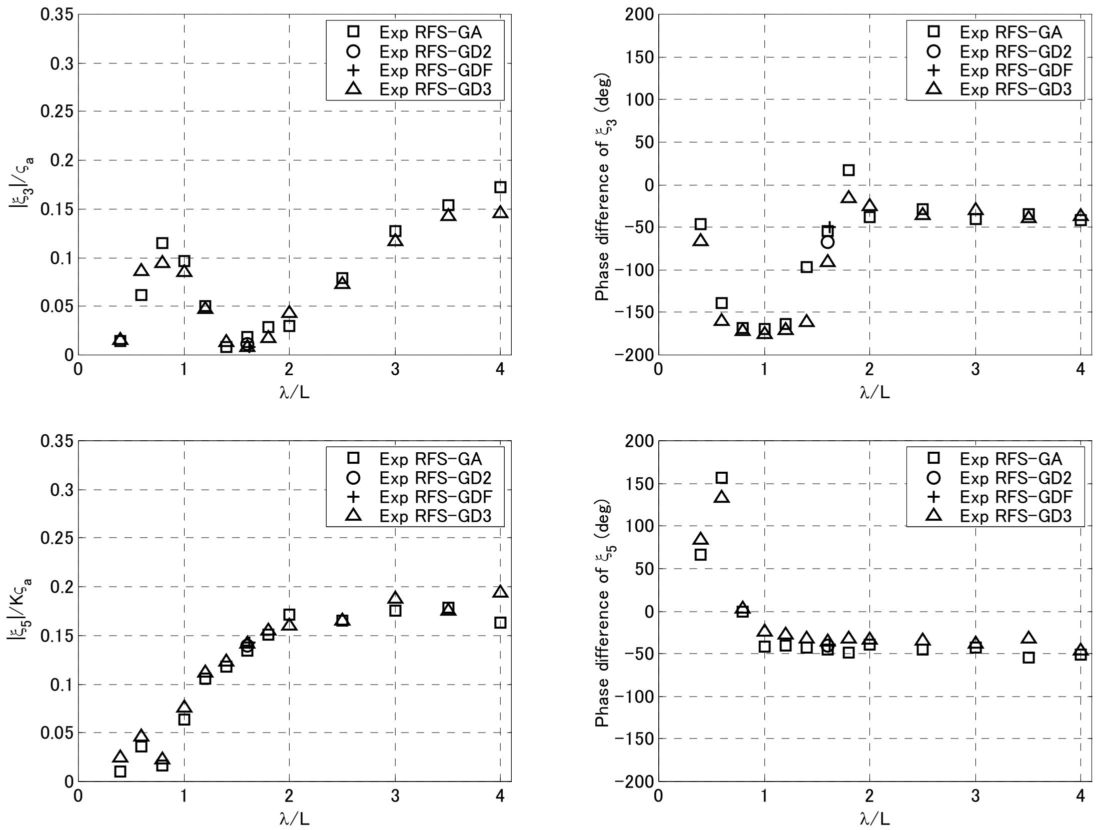

Figure 18: Effect of P gain on motion responses of RFS in regular head waves

Both results of the theoretical estimations and the experiments regarding the discriminant for the RFS model are described in Figure 15. In the figure, the symbol Est represents the simulation by using a Bode plot. Also the abscissa of gain rate indicates the magnification ratio of fundamental D gain constant as predicted in Table 3 while the ordinate denotes the control stability as described above. The value greater than 1.0 on the ordinate axis means that the control system is unstable. From Figure 15, it can be seen that the experimental results for the RFS agree well with the theoretical estimations. Accordingly, it is confirmed that the maximum stable D gain for the RFS model equals gain rate of 1.0.

The same experiments to search the maximum stable gain for the ordinary SWATH model have also been carried out. The experimental results for the ordinary SWATH are described in Figure 15. It can be observed that gain rate 0.6 is the maximum stable D gain for the ordinary SWATH model.

The reason to choose the different values of gain rate, i.e. 1.0 and 0.6 for these two hull forms, arises from the fact that the energy accumulated by the attack angle of the fin is dissipated easily in the case of the RFS because of the large damping coefficients of the ship hull compared with those of the ordinary SWATH.

6. MOTION RESPONSES

6.1 EFFECT OF 'P' GAIN OR 'D' GAIN

The effect of P gain or D gain on the motion responses of the ordinary SWATH model or the RFS model advancing at F_n = 0.433 in regular head waves has been examined in the experiments in detail. In the experiments of the motion responses, fundamental PD gain constants adopted for the ordinary SWATH model or the RFS model are shown in Table 4. In the table, the symbol OGA, in which D gain rate equals 0.6, indicates the gain constants for the ordinary SWATH model while the symbol GA, in which D gain rate is 1.0, denotes the gain constants for the RFS model, where the P gain constant of the pitch motion for the ordinary SWATH model is adopted as K_{P5}=0 because the ordinary SWATH model has enough positive restoring moments.

Firstly, the experimental results regarding the effect of D gain on the motion responses of the ordinary SWATH are shown in Figure 16. The gain constants tested in the experiments are listed in Table 5. In the table, the symbols OGA, OGC2 and OGC indicate gain rate 0.6, 0.8 and 1.0 respectively. The experiments in the case of OGC2 or OGC have been forced to continue regardless of the fluctuation of the attack angle. In the figure, the abbreviation Ord stands for the ordinary SWATH with fixed fins which is not controlled by PD and the symbol Strip denotes the calculated results by means of strip method. It is observed that the heave and pitch motion responses of the ordinary SWATH is reduced considerably by using D control gain and the effect of that is saturating near gain OGA, and also the phase differences of the motions in the experiments agree well with each other.

Secondly, the experimental results regarding the effect of D gain on the motion responses of the RFS are presented in Figure 17 and the gain constants tested are listed in Table 6. In the table, the symbols GB, GA and GC denote gain rate 0.5, 1.0 and 1.2 respectively. Also the experiments in the case of gain GC have been forced to go on in spite of the fluctuation of the attack angle. It can be seen that the effect of D gain on the reduction of the heave and pitch motion responses is obvious, and the effect of that is saturating near gain GA. Moreover, the phase differences of the motions in the experiments agree well with each other. From these results, it can be concluded that the experiments are carried out with high accuracy.

Thirdly, the experimental results regarding the effect of P gain constants on the motion responses of the RFS are shown in Figure 18 and the gain constants tested are listed in Table 7, where the symbol GD2, GDF or GD3 has the P gain constant of 2.0, 2.4 or 3.0 times as much as the P gain constant of GA. It can be seen from the figure that there is no significant effect of P gain constant on the heave and pitch motion responses.

Accordingly, it is understood that the policy to adopt the PD gain constants described previously, i.e. the minimum P gain and the maximum D gain should be selected, is correct.

6.2 MOTION RESPONSES IN REGULAR WAVES

The experiments to compare the motion responses in regular head waves among four hull forms, i.e. the mono-hull, the ordinary SWATH, the trimaran and the RFS, have been carried out.

The experimental and theoretical results of the heave and pitch motion responses of four hull forms in regular head waves are presented in Figure 19. Gains of OGA for the ordinary SWATH model and GA for the RFS model shown in Table 4 have been adopted in the experiments. The calculated results for the mono-hull and the trimaran models by the use of RPM are presented in the figure. The results of the theoretical estimation for the RFS by the use of RNM are also plotted in the same figure, where the abbreviation RNM indicates the method that the hydrodynamic coefficients and the wave exciting forces used in the motion equations of the theoretical study are replaced i.e. renormalized by the experimental measurements.

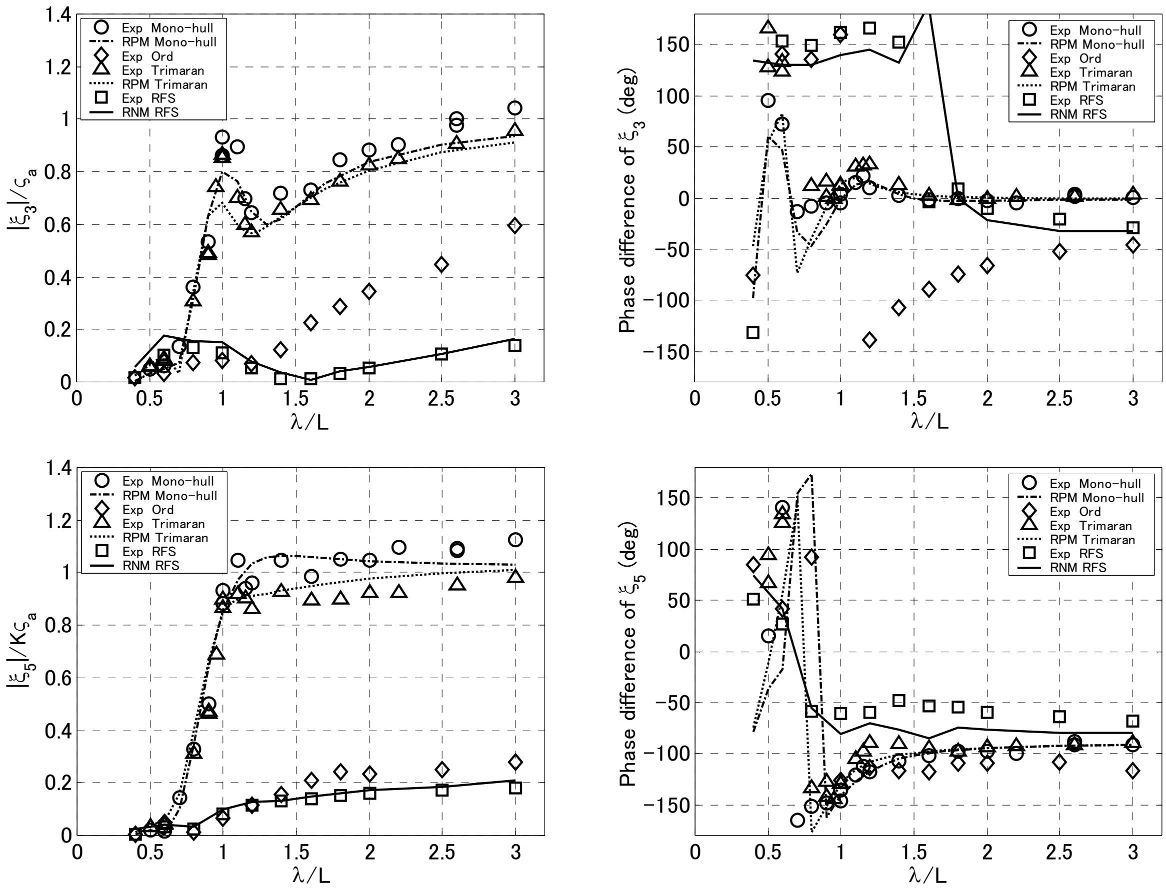

Figure 19: Motion responses of four kinds of hull forms in regular head waves

Firstly, it is observed that the calculated or the estimated results coincide very well with the experimental results. Accordingly, it can be understood that the design policy of PD control system for the motions of the RFS is valid in the present theory.

Secondly, in comparison among the mono-hull, the trimaran and the RFS, the heave and pitch motion responses of the RFS are significantly smaller than those of two other hull forms. An obvious resonant peak exists in the motion responses of the mono-hull, the trimaran near λ/L = 1.0 but this is not so evident for the ordinary SWATH. In the case of the RFS, there is no resonance at all.

Thirdly, in the comparison between the ordinary SWATH and the RFS, i.e. the same SWATH models with different strut length, it is observed that the motion responses of the RFS are much smaller in the heave motion and are smaller in the pitch motion than those of the ordinary SWATH. The difference between the motions of the ordinary SWATH and the RFS may be attributed to the advantages of the RFS: such as no resonant peak, the small wave exciting forces, the large damping coefficients of hull and the large D gain which can be adopted for the RFS.

6.3 INDEXES OF SEAWORTHINESS FOR RFS

The theoretical estimation of seaworthiness properties for the RFS running at 40 knots in regular head waves with 8 m wave height in real scale is presented in Figure 20. The figures are numbered from the top. The first figure shows the amplitude of the attack angle, including the angle of incident flow, of the fore or aft fin. The results of those are less than 20 deg i.e. less than the stall angle. The second and third figure shows the motions of the fins or the bow relative to the wave surface. The relative distance between these positions and the water surface equals 8.425 m in still water. It can be seen that the relative displacement decreases this distance to almost half but no further. This ensures that there is sufficient safety for no slamming or propeller racing even in a sea state with 8 m wave height. The fourth figure shows the vertical acceleration at the bow. It is observed that the acceleration is less than 0.1-0.2 G. As expected, the RFS is the less-oscillating ship in the rough sea.

Next, the comparison of the added resistance in waves between the existing mono-hull ship and the RFS is shown in Figure 21. The experimental results of the typical container ship [17], having 300 m length, 40 m breadth, approximately 100,000 displacement tonnage and F_n = 0.247, are adopted for the mono-hull. It is observed that the added resistance in waves of the RFS is much smaller than that of the existing container ship because the motion responses of the RFS are greatly reduced. Consequently, the sea margin for the RFS can be reduced, which leads to an increased transport and economical efficiency of the RFS compared to those of the existing ships, including the fuel efficiency, the punctuality and the damage for the cargo.

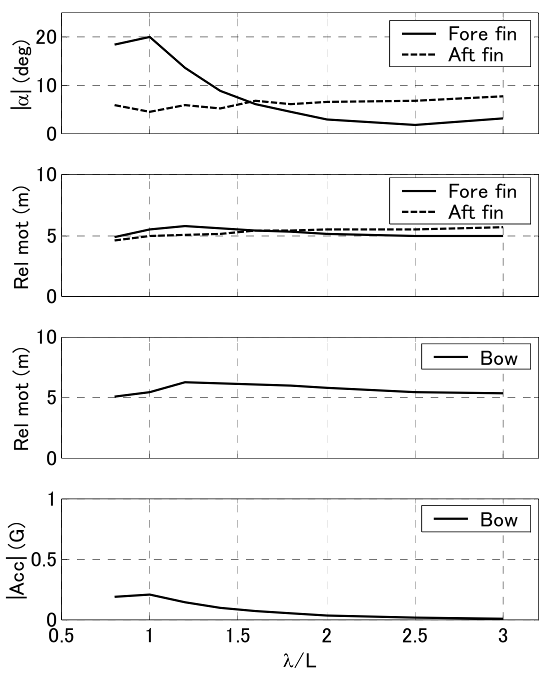

Figure 20: Seakeeping properties of RFS running at 40 knots in regular head waves with 8 m wave height

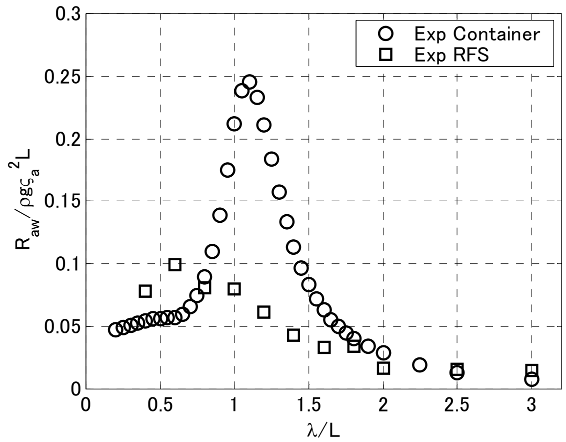

Figure 21: Added resistance in regular head waves

6.4 MOTION RESPONSES IN IRREGULAR WAVES

The experimental and estimated results of the heave and pitch motion responses of the ordinary SWATH and the RFS models running at F_n=0.433 in irregular head waves are presented in Figure 22 through 25. Gains of OGA for the ordinary SWATH model and GA for the RFS model have been adopted in the experiments.

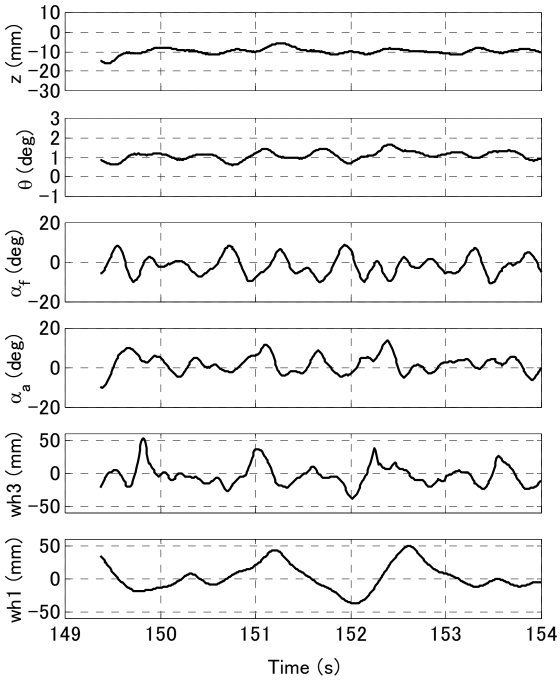

Figure 22: Seakeeping properties of RFS measured in irregular head waves

In Figure 22 the six small figures are numbered from the top. The first and second figure shows the motion displacement of heave z or pitch θ respectively. It can be seen that the RFS model is very stable with PD control in big irregular waves with up to 10 m wave height in real scale. There is absolutely no observation of slamming, propeller racing, green water or wet-deck slamming on the underside of the upper deck. The third and fourth figure shows the results of the attack angle of the fore or aft fins respectively. The amplitude of the attack angles is less than 10 deg and it can be concluded that PD control works well for the RFS model. The fifth and sixth figure shows the wave height measured at the meter *wh3* following the motion of the model or the fixed meter *wh1*.

Secondly, the wave spectrum measured at the fixed wave meter *wh1* is shown in Figure 23 and the result of spectrum analysis is described in Table 8. It is observed that the measured results coincide well with the aimed ISSC wave spectrum with a significant wave height of 0.071 m and a mean wave period of 1.23 sec. Also, the wave spectrum measured at the moving wave meter *wh3* is shown in Figure 24 and the result of spectrum analysis is described in Table 9. The measured result coincides generally well with the target ISSC spectrum. While the number of encounter wave components used to recreate the spectra equals 350 approximately.

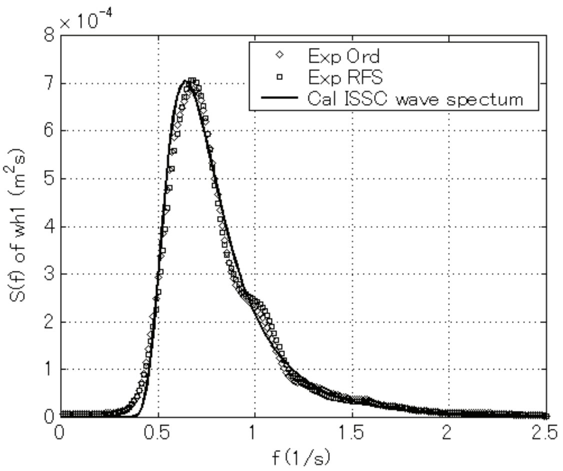

Figure 23: Wave spectra of *wh1* (fixed)

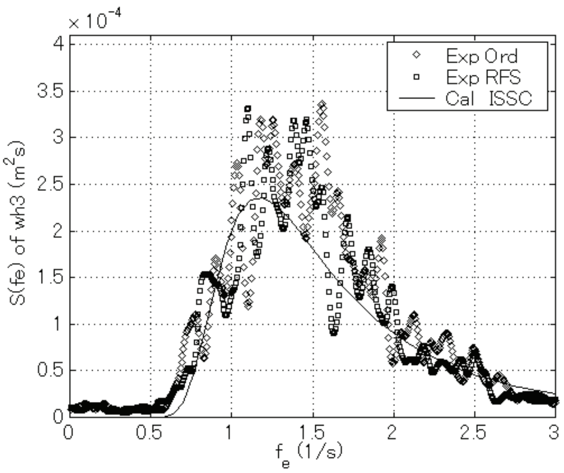

Figure 24: Wave spectra of *wh3* (F_n=0.433)

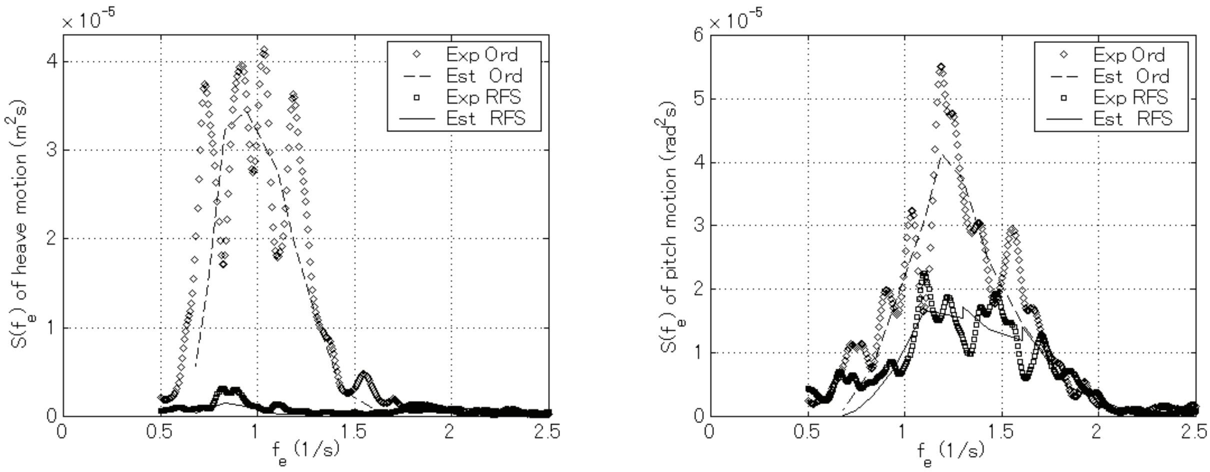

Figure 25: Heave and pitch motion spectra of ordinary SWATH and RFS running at F_n=0.433 in head waves

Table 8: Spectrum analysis of *wh1* (fixed)

Spectrum	$m_0=\sigma^2$ (m²)	$H_{1/3}$ (m)	T_{01} (s)
Exp Ord	3.163*10⁻⁴	0.071	1.23
Exp RFS	3.154*10⁻⁴	0.071	1.23
Cal ISSC	3.140*10⁻⁴	0.071	1.23

Table 9: Spectrum analysis of *wh3* (F_n=0.433)

Spectrum	$m_0=\sigma^2$ (m²)	$H_{1/3}$ (m)	T_{01} (s)
Exp Ord	2.99*10⁻⁴	0.069	---
Exp RFS	2.76*10⁻⁴	0.067	---
Cal ISSC	2.89*10⁻⁴	0.068	1.2

Table 10: Spectrum analysis of motion responses

Spectrum	Heave z		Pitch θ	
	$m_0=\sigma^2$ (m²)	$z_{1/3}$ (m)	$m_0=\sigma^2$ (m²)	$\theta_{1/3}$ (rad)
Exp Ord	0.214*10⁻⁴	0.01854	0.284*10⁻⁴	0.000213
Exp RFS	0.016*10⁻⁴	0.00514	0.156*10⁻⁴	0.000158

Thirdly, the measured and estimated spectra of the heave or pitch motion for the ordinary SWATH and the RFS models are illustrated in Figure 25 and the result of spectrum analysis is shown in Table 10. In the figure, the symbol Est indicates the estimated result, which is calculated by a combination of the measured response amplitude operator in regular waves as shown in Figure 19 and the analytical ISSC spectrum. It can be seen that the measured spectra in the heave and pitch motions coincide very well with the estimated spectra in both cases of the ordinary SWATH and the RFS. Also it is confirmed that the motion responses of the RFS are

©2014: The Royal Institution of Naval Architects

reduced extremely in the heave motion and they are reduced considerably in the pitch motion compared with those of the ordinary SWATH.

6.5 SUMMARY OF MOTION RESPONSES

The theoretical and experimental results of the motion responses in regular and irregular head waves are summarized in Table 11.

Table 11: Comparison of motion responses

	Max. wave energy, λ/L=1.6		Important range, λ/L=1.0–2.0		Exp. max. 1/1000, irregular $H_{1/3}$=8 m	
	Heave	Pitch	Heave	Pitch	Heave	Pitch
Mono-hull Trimaran	60	8	22	8	---	---
Ordinary SWATH	19	1.5	5	1.4	4	1.4
RFS	1	1	1	1	1	1

Firstly, considering the case of a ISSC wave spectrum with the significant wave height of 8 m and the mean wave period of 12 s in real ship scale, the wave period T_P with the maximum energy corresponds to a wave length λ/L=1.6 approximately. The results of the motion responses for four kinds of hull forms described in Figure 19 are compared in the second column from the left of Table 11. It can be seen from the table that the heave motion for the RFS equals 1/60 compared to that of the mono-hull or the trimaran while the pitch motion equals 1/8. Also, in comparison with the ordinary SWATH, the heave motion of the RFS is 1/19 while the pitch motion of the RFS is 2/3 as that of the ordinary SWATH.

Secondly, it can be recognized that the most important range of the wave length for the motion responses is λ/L=1.0–2.0 (λ = 230–460 m) in Figure 19 from the aspect of the ocean wave statistics at North Atlantic Ocean in winter by Walden [18], so the comparison of the average motion responses within λ/L=1.0–2.0 among four hull forms is described in the third column of Table 11. It is observed that the motion responses of the RFS are greatly reduced compared with other hull forms in the same manner.

Thirdly, the comparison of the results obtained from the analysis of the motion spectra in irregular waves with the significant wave height of 8 m is described in the fourth column of Table 11. The expected maximum value of the motion response out of 1,000 waves in the case of the RFS is reduced to 1/4 in the heave motion while almost 2/3 in the pitch motion compared with that of the ordinary SWATH.

In conclusion, the heave and pitch motion responses of the RFS are significantly reduced compared with other hull forms such as the mono-hull, the ordinary SWATH and the trimaran.

7. CONCLUSIONS

The theoretical estimations and the experiments regarding the linear PD control have been carried out to minimize the motion responses of the RFS and the results have been compared with other hull forms.

Firstly, regarding PD control of the RFS motions by using the fin-generated lift: the motion equations have been formulated to include the controlling forces due to the fin-generated lift. The unsteady characteristics of the lift, such as the time lag in the lift generation and the interaction among the fins and the lower hulls, and the time lag of total control system are taken into account. Meanwhile, the hydrodynamic forces acting on the hull forms and the lift-curve slope of the fins have been obtained both by the experiments and the theoretical calculations.

Secondly, the Laplace transform has been applied to those motion equations and it is expressed as the block diagram of the control system. In this study, a two-step approach has been devised to obtain the open-loop transfer functions in the multi-input multi-output control system.

- Step 1, the control system is regarded as the single-input single-output system in which only pitch control works without any control on the heave motion.
- Step 2, the heave and pitch motions are both controlled. In this step, pitch gains are fixed at the constants decided at step 1 and pitch control is regarded as closed-loop. Then, the maximum stable D gain constants for the RFS are determined by using a Bode plot in the theoretical estimation.

The maximum stable D gain constants are also obtained from the results of the impulse response experiments in still water using the ordinary SWATH and the RFS models with controlling fins. The theoretical and experimental results agree well with each other.

Thirdly, the theoretical calculations and the experiments to measure the motion responses of the RFS in regular head waves using the proper control PD gains have been carried out. It is observed that the theoretical results coincide well with the experimental results, which confirms that the theoretical estimation including the unsteady characteristics of the fin-generated lift and the stability of the control system is reliable in this study. The motion responses of the RFS have been compared with those of other hull forms such as the mono-hull, the ordinary SWATH or the trimaran. The motion responses of the RFS are significantly reduced compared with those of the mono-hull and the trimaran, and considerably reduced compared with those of the ordinary SWATH.

Furthermore, the indexes of the seaworthiness of the RFS have been discussed. As the result, it can be recognized that those indexes for the RFS, such as the relative motion between the wave surface and the fin or the bow, the vertical acceleration at the bow and the added resistance in waves, are outstanding compared with those for other existing hull forms.

Finally, the motion responses of the RFS in irregular head waves have been compared with those of the ordinary SWATH. In the comparison of the power spectrum of the motion responses in irregular waves, the RFS shows the dominant properties of the seaworthiness compared with the ordinary SWATH.

8. ACKNOWLEDGEMENTS

This study has been performed by the assist of grant-in-aid for scientific research (No. 23246151), Japan Society for the Promotion of Science.

9. REFERENCES

1. TAKARADA, N., TAKEZAWA, S., HIRAYAMA, T., WANG, X., KOBAYASHI, K. and SAKURAI, H., R&D of a displacement-type high speed ship (Part 4: Seakeeping qualities in high speed range), *Journal of the Society of Naval Architects of Japan, Vol. 171, 73–82*, 1992.
2. PAPANIKOLAOU, A., ZARAPHONITIS, G. and ANDROULAKAKIS, M., Preliminary design of a high-speed SWATH passenger/car ferry, *Journal Marine Technology, SNAME, Vol. 28, No. 3, 129–141*, 1991.
3. HEARN, G. E., VELDHUIS, I. J. S., VEER, R. and STEENBERGEN, R. J., Conceptual design investigations of a very high speed transpacific container vessel, *6th International Conference on Fast Sea Transportation (FAST2001), 81–107*, 2001.
4. ARMSTRONG, T. and HOLDEN, K., A new generation of large fast ferry – from concept to contact reality, *7th International Conference on Fast Sea Transportation (FAST2003), 75–84,* 2003.
5. DUDSON, E. and GEE, N., Optimisation of the Seakeeping and Performance of a 40 knot Pentamaran Container Vessel, *6th International Conference on Fast Sea Transportation (FAST 2001)*, 2001.
6. LEE, C. M., Theoretical prediction of motion of Small-Waterplane-Area, Twin-Hull (SWATH) ships in waves, *DTNSRDC Report, SPD–76–0046*, 1976.
7. LEE, C. M. and CURPHEY, M., Prediction of motion, stability, and wave load of Small-Waterplane-Area Twin-Hull Ships, *SNAME Transactions*, *Vol. 85*, *9–4130*, 1977.
8. MATSUSHIMA, M., NAKAMURA, H. and KUNITAKE Y., Seakeeping of A Semi-Submerged Catamaran (SSC) Vessel, *Transactions of the West-Japan Society of Naval Architects, Vol. 63, 97–114,* 1982.
9. KYOZUKA, Y., HORI, T. and KOTERAYAMA, W., Unsteady Hydrodynamic Forces on a Lifting Body (Second Report, Interaction of Lift between Body and Wing), *Journal of the Society of Naval Architects of Japan, Vol. 168*, *243–251*, 1990.
10. YOSHIDA, T., FUJITA, Y. and FUJINO, M., A proposal of the CS-Swath as a Transocean High Speed Ship, *Transactions of RINA*, *Vol.142 (B)*, *136–149*, 2000.
11. YOSHIDA, T., Semi-submerged twin hull ship, *British patent GB2,332,174*, 1999.
12. YOSHIDA, M., KIHARA, H., IWASHITA, H. and KINOSHITA, T., On the Resonance-Motion-Free SWATH as an oceangoing large fast ship, *International conference on innovation in high speed marine vessels*, *31–38*, 2009.
13. ELANGOVAN, M., IWASHITA, H., SAITO, H. and ITO, A., Seakeeping Estimations of Fast Ships with Transom Stern, *Journal of the Japan Society of Naval Architects and Ocean Engineers, Vol. 7, 195–206*, 2008.
14. KIHARA, H., YOSHIDA, M., IWASHITA, H. and KINOSHITA, T., Motion response analysis for a Resonance-Free SWATH, *Journal of the Japan Society of Naval Architects and Ocean Engineers, Vol. 10, 83–96*, 2010.
15. PITTS, W. C., NIELSEN, J. N. and KAATTARI, G. E., Lift and center of pressure of wing-body-tail combinations at subsonic, transonic, and supersonic speeds, *National Advisory Committee for Aeronautics*, *Report 1307*, 1959.
16. WHICKER, L. F. and FAHLNER, L. F., Free-Stream Characteristics of a Family of Low-Aspect-Ratio, All-Movable Control Surfaces for Application to Ship Design, *David Taylor Model Basin Report 933*, 1958.
17. TSUJIMOTO, M., SHIBATA, K. and KURODA, M., A Practical Correction Method for Added Resistance in Waves, *Journal of the Japan Society of Naval Architects and Ocean Engineers, Vol. 8, 177–184*, 2008.
18. WALDEN, H., Die Eigenschaften der Meerswellen im Nordatlantischen Ozean, *Deutscher Wetterdienst, Seewetteramt, Einzerveröffentlichungen, Nr. 41, Hamburg,* 1964.

©2014: The Royal Institution of Naval Architects